Solvent Effect of Room Temperature Ionic Liquids on Electrochemical Reactions in Lithium–Sulfur Batteries

ARTICLE *in* THE JOURNAL OF PHYSICAL CHEMISTRY C · FEBRUARY 2013

Impact Factor: 4.77 · DOI: 10.1021/jp400153m

THE JOURNAL OF PHYSICAL CHEMISTRY C

Article

pubs.acs.org/JPCC

Solvent Effect of Room Temperature Ionic Liquids on Electrochemical Reactions in Lithium−Sulfur Batteries

Jun-Woo Park, Kento Yamauchi, Eriko Takashima, Naoki Tachikawa, Kazuhide Ueno, Kaoru Dokko, and Masayoshi Watanabe*

Department of Chemistry and Biotechnology, Yokohama National University, 79-5 Tokiwadai, Hodogaya-ku, Yokohama 240-8501, Japan

Supporting Information

ABSTRACT: A room temperature ionic liquid (RTIL), *N*,*N*-diethyl-*N*-methyl-*N*-(2-methoxyethyl)ammonium bis(trifluoromethanesulfonyl)amide ([DEME][TFSA]), was used as an electrolyte solvent for lithium−sulfur (Li−S) batteries. Li[TFSA] was dissolved into [DEME][TFSA] to prepare the electrolytes, and a molecular solvent—tetraethylene glycol dimethyl ether (TEGDME)—was used for Li[TFSA] as a reference. Discharge−charge tests of Li−S cells using these electrolytes were carried out. The discharge−charge cycle stability and Coulombic efficiency of a cell with an RTIL electrolyte were found to be surprisingly superior to those of a cell with TEGDME electrolyte. The poor cycle stability of the cell with the TEGDME electrolyte was attributed to the dissolution of lithium polysulfides (Li_2S_m), which were generated as reaction intermediates through a redox process at the S cathode in the Li−S cell. RTIL has low donor ability owing to the weak Lewis basicity of $[TFSA]^-$ anion, whereas conventional ether-based molecular solvents such as TEGDME have high donor ability. The dissolution of Li_2S_m was significantly suppressed owing to the weak donor ability of RTIL. In the RTIL electrolyte, Li_2S_m was immobilized on the electrode, and the electrochemical reaction of the S species occurred exclusively in the solid phase. These results clearly prove a novel solvent effect of RTILs on the electrochemical reactions of the S cathode in Li−S cells.

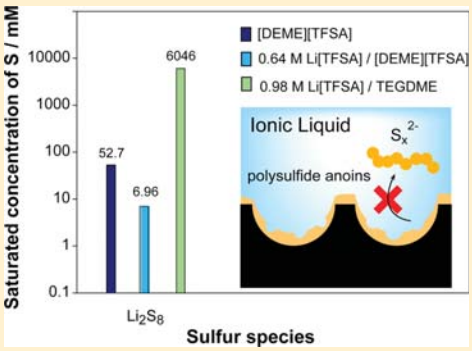

INTRODUCTION

Lithium−sulfur (Li−S) batteries have attracted a great deal of attention as the next-generation energy-storage devices.[1,2] Elemental sulfur (S_8) has a high theoretical capacity of 1672 mA h g^{-1}, which is ∼10 times larger than that of conventional cathode materials used in lithium batteries, such as $LiCoO_2$ and $LiFePO_4$. Therefore, the use of a S cathode can dramatically increase the energy density of lithium batteries. There have been many reports on Li−S batteries;[3−8] however, cells using S cathode generally suffer from low active-material utilization and rapid capacity fading with charge−discharge cycles. A poor charge−discharge performance may result from the insulating nature of the S compound,[6,7] sluggish redox kinetics,[7] and the dissolution of lithium polysulfides (Li_2S_m: $2 \le m \le 8$).[8] Lithium polysulfides are reaction intermediates formed through redox process at the S cathode, and they are easily dissolved into conventional ether-based liquid electrolytes, which are frequently used as solvents due to the stability to the polysulfide ions and lithium electrode.

Nazar et al. recently reported that a nanocomposite electrode, consisting of three-dimensionally ordered porous C and S, can greatly improve the charge−discharge performance of Li−S cells.[9−11] The intimate contact between porous C and S is believed to secure the collection of current from the electrochemically active but insulating S, resulting in high utilization of S in the cathode. Furthermore, the high specific surface area of porous C was found to be effective for adsorbing Li_2S_m and preventing it from diffusing into the bulk electrolyte. The design of the electrolyte composition is also an important factor. Solid electrolytes consisting of polymers or inorganic solids have been used as physical barriers for inhibiting the dissolution of Li_2S_m.[12−17] Although solid electrolytes have beneficial properties, many difficulties still remain in forming a favorable solid-electrolyte/solid-electrode interface for electrochemical reactions. In the case of liquid electrolytes, considerable effort has been devoted to the optimization of the particular organic solvent used to achieve high utilization of active material and promote electrode kinetics.[18−26] Ether-based solvents have been most commonly researched. In this case, the aforementioned dissolution of Li_2S_m into an electrolyte is caused by the high donating ability of the solvents such as tetrahydrofuran (THF), 1,3-dioxolane (DOL), and dimethoxyethane (DME), which are usually used to dissolve Li salts.[18−21] The dissolved Li_2S_m can react directly with the Li metal anode, leading to low charge−discharge Coulombic efficiency.[8] The addition of $LiNO_3$ into the electrolyte was reported to be effective in preventing this direct reaction between Li_2S_m and Li metal because $LiNO_3$ generates a

Received: January 5, 2013
Revised: February 9, 2013
Published: February 12, 2013

   dx.doi.org/10.1021/jp400153m | J. Phys. Chem. C 2013, 117, 4431−4440

protective film composed of Li_xNO_y and Li_xSO_y onto the surface of the Li metal anode.[23,24] However, the repetition of charge−discharge cycle may destroy the protective film. Further developments are seriously required to solve these problems and achieve better Coulombic efficiency, higher power density, and longer cycle life of Li−S batteries.

In the present study, we focus on the use of room temperature ionic liquids (RTILs) as alternative solvents for electrolytes in Li−S batteries. RTILs consist entirely of cations and anions and have relatively low melting points (<100 °C), negligible volatility, and reasonably high ionic conductivity. In addition, they remain in liquid form over a wide temperature range and are nonflammable.[27−31] Extensive researches into the utilization of RTILs as thermally stable electrolytes for electrochemical devices have been conducted. Aprotic RTILs have been specifically studied as electrolytes for use in electrochemical capacitors,[32−35] dye-sensitized solar cells,[36−38] and lithium batteries.[39−47] Typical aprotic RTILs are composed of weakly Lewis acidic cations (such as imidazolium cations and quaternary ammonium cations) and weakly Lewis basic anions (such as BF_4^- and PF_6^-),[48−52] whereas conventional organic molecular solvents of battery electrolytes, such as THF, DOL, and DME, have a relatively strong Lewis basicity. It has been anticipated that the weakly Lewis acidic/basic nature of RTILs results in weak interactions of the cations and/or anions with Li_2S_m. An exploration and comparison of the electrochemical reaction mechanisms of S cathode in electrolytes with RTILs and molecular solvents are of great interest.

A typical RTIL, *N*,*N*-diethyl-*N*-methyl-*N*-(2-methoxyethyl)-ammonium bis(trifluoromethanesulfonyl)amide ([DEME][TFSA]) was used as an electrolyte solvent. We have reported the physicochemical and electrochemical properties of binary ionic liquid Li[TFSA]/[DEME][TFSA][46] and stable operation of a Li−$LiCoO_2$ cell using Li[TFSA]/[DEME][TFSA] as the electrolyte.[47] Tetraethylene glycol dimethyl ether (TEGDME) with a chemical structure of $CH_3-O-(CH_2-CH_2-O)_4-CH_3$ was also used as a typical molecular electrolyte solvent.[47] TEGDME has a relatively high donor number (DN) and preferably coordinates with Li^+ cations.[53−62] The detailed physicochemical properties of Li[TFSA]/TEGDME solution have been reported elsewhere.[63−66] In this work, the performances of Li−S battery using electrolytes with an RTIL solvent and a molecular solvent were evaluated. The charge−discharge stability of a battery dramatically changes depending on the type of electrolyte solvent used. The solubility of Li_2S_m in an electrolyte was evaluated quantitatively, and the reaction mechanisms of S cathode were investigated in detail.

EXPERIMENTAL SECTION

Electrolytes. Li[TFSA] (Morita Chemical Industries Co., Ltd.) was dried under vacuum at 80 °C for 12 h prior to use. [DEME][TFSA] was purchased from Kanto Chemical and used as received. Highly pure TEGDME (Nippon Nyukazai Co., Ltd.) was also used as received. To prepare the electrolytes, Li[TFSA] was dissolved into [DEME][TFSA] or TEGDME. The compositions of the electrolytes are listed in Table 1. The water content in the electrolytes was <30 ppm, as evaluated through Karl Fisher titration (Mitsubishi CA-07). The electrolytes were stored and handled in an argon-filled glovebox (VAC, dew point < −80 °C). The ionic conductivities of the electrolytes were determined through complex impedance method using an ac impedance analyzer (Princeton Applied Research, VMP2) in the frequency range of 500 kHz to 1 Hz with a sinusoidal alternating voltage amplitude of 10 mV root-mean-square. A cell equipped with two platinized Pt electrodes was utilized for conductivity measurements (TOA Electronics, CG-511B), and the cell constant was determined based on a standard 0.01 mol dm^{-3} KCl aqueous solution (Kanto Chemical) at 25 °C. The viscosity and density of the electrolytes were measured using an SVM3000 (Anton Paar). The Lewis basicity of electrolytes was evaluated from the maximum ultraviolet−visible (UV−vis) absorption wavelength (λ_{Cu}) of a copper complex solvatochromic probe, (acetylacetonate)(*N*,*N*,*N*′,*N*′-tetramethylethylenediamine)-copper(II) tetraphenylborate, [Cu(acac)(tmen)][BPh_4],[67] dissolved in electrolytes.

Table 1. Density (d), Viscosity (η), and Ionic Conductivity (σ) of Electrolytes at 30 °C

electrolyte	d/g cm^{-3}	η/mPa s	σ/mS cm^{-1}
[DEME][TFSA]	1.41	57.5	3.44
0.64 M Li[TFSA]/[DEME][TFSA]	1.46	117	1.30
0.98 M Li[TFSA]/TEGDME	1.16	9.66	3.22

Carbon/Sulfur Composite Electrode. Ketjen black (KB, Lion Corporation), a porous C with high specific surface area of 1270 m^2 g^{-1}, was used as a substrate for S. KB and S_8 (Wako Pure Chemical Industries) were mixed using an agitating mortar, and the mixture was transferred to a vial and kept at 155 °C for 6 h, according to a method reported by Nazar et al.[9] During the heat treatment, S_8 melted and diffused into the pores of KB. To prepare the porous composite electrode, the C/S composite was mixed with poly(vinyl alcohol) (PVA) (degree of polymerization, 3100−3900; saponification degree, 86−90 mol %, Wako Pure Chemical Industries). Prior to mixing, PVA was dissolved in *N*-methylpyrrolidone (NMP) at an elevated temperature of 100 °C and subsequently cooled to RT. The C/S composite and PVA/NMP solution were mixed to form a slurry, which was then applied to an Al foil current collector. The slurry was dried in a drying oven at 80 °C for 12 h. The prepared composite sheet was cut into a circular shape (16 mm diameter) and compressed at 100 kgf cm^{-2} using a hydraulic press. The mass ratio of S/KB/PVA was controlled to 60:30:10. The thickness of the composite sheet on the Al was ca. 15 μm, and the mass of S on the sheet electrode was ca. 1.2 mg. A coin cell (2032 type) was fabricated in a glovebox using a porous composite cathode sheet, a porous glass separator (GA 55, Advantec), a Li foil anode, and an electrolyte. The electrolyte penetrated into the voids of the porous separator during the cell fabrication. The galvanostatic charge−discharge measurements of the Li−S cells were conducted using BTS-2004 (Nagano). The charge−discharge measurements were carried out within 1.5−3.3 V range at 30 °C.

A galvanostatic intermittent titration technique (GITT) was carried out for the Li−S cell using VMP2 (Princeton Applied Research) at 30 °C. The cell was discharged or charged at a constant current density of 139 mA g^{-1} sulfur for 10 min; the current supply was then interrupted, and the cell voltage relaxation was monitored until the voltage change became <15 mV h^{-1}. The voltage at the end of the relaxation was defined as an open-circuit voltage (OCV). The galvanostatic titration was repeated until the OCV reached the cutoff voltage (1.5 V for the discharging process and 3.3 V for the charging process). When the cell reached the cutoff voltage during the galvanostatic titration, the cell was successively discharged or charged at the cutoff voltage for 20 min, or until the current

dx.doi.org/10.1021/jp400153m | J. Phys. Chem. C 2013, 117, 4431−4440

declined to less than 13.9 mA g^{-1} sulfur, and OCV was then measured.

To identify the electrochemically generated Li_2S, the Li−S cells were disassembled at various discharged or charged states, and the S electrodes were subjected to X-ray diffraction (XRD) measurements (RINT-2000, Rigaku) with Cu Kα radiation. The disassembly of the cell was carried out in an Ar-filled glovebox to avoid the moisture reaction of Li_2S. The electrode was tightly wrapped with a 30 μm thick polyethylene (PE) film to avoid any exposure to air during the XRD measurements.

Solubility Measurements of S_8 and Li_2S_m. The solubility of S_8 in the electrolytes was determined using UV−vis spectroscopic measurements (UV-2500PC, Shimadzu). The absorbance at 266 nm correlated linearly with the concentrations of S_8, and the solubility of S_8 in the electrolytes was easily quantified. An excessive amount of S_8 was mixed with the electrolytes at 60 °C for 100 h with vigorous stirring and then kept at 30 °C for 48 h without stirring. UV−vis measurements were then carried out for the supernatant electrolytes saturated with S_8.

The solubility of Li_2S_m in the electrolytes was measured as follows. S_8 and Li_2S powders (Aldrich) were mixed in various ratios using an agitating mortar in an Ar-filled glovebox. The mixed powder was placed in a vial containing an electrolyte and maintained at 60 °C for 100 h with stirring. Li_2S_m was generated during the stirring owing to the direct reaction of Li_2S with S_8 ($8Li_2S + (m - 1)S_8 \rightarrow 8Li_2S_m$);[68] the electrolyte was then maintained at 30 °C for 48 h without stirring. The electrolyte was considered to be saturated with Li_2S_m owing to the precipitation observed at the vial bottom. The supernatant liquid saturated with Li_2S_m was diluted with a known amount of TEGDME, and Li_2S_m in the diluted solution was electrochemically oxidized to S_8 using a two-electrode system in a two-compartment cell. A carbon felt electrode was used for the working electrode; the counter electrode was made of Li metal, which was placed in a compartment separated from the working electrode with a glass filter. The potentiostatic oxidation was performed at a cell voltage of 3.0 V for 12 h with stirring. Through electrolysis, S_m^{2-} was oxidized to S_8 at the carbon felt electrode, and the concentration of S_8 in the electrolyte was then determined using a UV−vis measurement, as already mentioned. The UV−vis spectrum of the oxidized sample showed a characteristic shape corresponding to S_8 without the peaks of Li_2S_m. To check the validity of this analysis method, a Li_2S_m solution with a known concentration (24 mM atomic concentration of S, obtained through a reaction between 3 mM Li_2S and 2.625 mM S_8) dissolved in 0.98 M Li[TFSA]/TEGDME was prepared and analyzed. The analytically determined concentration of S in the solution was 23.44 ± 0.64 mM and showed good reproducibility and agreement with the prescribed concentration of Li_2S_m.

RESULTS AND DISCUSSION

Physicochemical Properties of Electrolytes. Table 1 shows the density (d), viscosity (η), and ionic conductivity (σ) of the electrolytes at 30 °C. The physicochemical and electrochemical properties of binary ionic liquid Li[TFSA]/[DEME][TFSA] were reported elsewhere.[46] Li[TFSA] can be dissolved into [DEME][TFSA] in a wide range of concentrations. By dissolving Li[TFSA] into [DEME][TFSA], the coordination of Li^+ cations with two $[TFSA]^-$ anions and the formation of Li(I) oligomeric species were reported to occur owing to the strong Lewis acidity of Li^+ cations.[69,70] The complex formation of such structures has brought about an increase in the viscosity and a decrease in the ionic conductivity (Table 1). A concentration of 0.64 M Li[TFSA] in [DEME]-[TFSA] was chosen because the Li(I) diffusion flux in the electrolyte reaches a maximum level at around 0.64 M, and the highest limiting current density can be achieved in a binary ionic liquid.[46] The physicochemical properties of Li[TFSA]/TEGDME solution were also previously reported.[64] The molar ratio of Li[TFSA]:TEGDME is 1:4 in 0.98 M Li[TFSA]/TEGDME solution. The ionic conductivity of Li[TFSA]/TEGDME solution changes depending on the Li[TFSA] concentration and reaches a maximum at ca. 1 M.

Dependence of Charge−Discharge Cycle Stability of Li−S Cell on Electrolyte Composition. Coin-type Li−S cells were fabricated to evaluate the feasibility of the electrolytes with an elemental S cathode. KB can retain a relatively large amount of S within its pores. The cell was prepared in a fully charged state, and the charge−discharge cycle is defined as follows: first discharge → second charge → second discharge → third charge → third discharge, and so forth. The Coulombic efficiency can be defined as (Nth discharge capacity)/(Nth charge capacity). The specific capacity of the cell was calculated based on the mass of S_8. Based on the mass of S_8, the gravimetric current density of 1672 mA g^{-1} was defined as 1C rate, which corresponds to a geometric current density of 1 mA cm^{-2}.

Figure 1 shows the galvanostatic charge−discharge curves of Li−S cells with 0.64 M Li[TFSA]/[DEME][TFSA] and 0.98 M Li[TFSA]/TEGDME measured at a low current density. Each cell shows discharge curves with two voltage regions. The initial discharge capacity of each Li−S cell is within the range of 800−1000 mA h g^{-1}, corresponding to 50−60% of the theoretical capacity of elemental S. Sulfur usually has cyclic structure (S_8) and is expected to show a theoretical capacity of 1672 mA h g^{-1} if the following reduction proceeds completely:

$$S_8 + 16Li^+ + 16e^- \rightarrow 8Li_2S$$

Although the structure of the C/S composite electrode is not optimized, the gravimetric energy density of the Li−S cell based on the mass of C/S composite and Li metal can be estimated to be 835 Wh kg^{-1}, which is much higher than that of a conventional cathode (Li−$LiCoO_2$) cell (415 Wh kg^{-1}). However, the volumetric energy density of the Li−S cell with the present C/S composite electrode is estimated to be 537 Wh L^{-1}, which is lower than that of the Li−$LiCoO_2$ cell (870 Wh L^{-1}) (see Supporting Information). To achieve higher volumetric energy density of a Li−S battery, the sulfur utilization in the C/S composite electrode should be enhanced. Actually, the discharge capacity shown in Figure 1 is lower than the previously reported value by Nazar's group.[9−11] The reason for the relatively low sulfur utilization in the C/S composite electrode is discussed later in this article. In addition to the sulfur utilization in the cell, the porosity of C/S composite electrode affects the volumetric energy density (see Supporting Information). In any case, the optimization of porous structure of C/S composite is important to increase the energy density of Li−S cells. For example, the use of three-dimensionally ordered macroporous or mesoporous carbon with an optimized pore size and specific surface area as a substrate for S may be effective in enhancing the sulfur utilization in the cell,[66] as was demonstrated previously.

Although the exact electrochemical reaction mechanism for S has yet to be identified, the voltage-sloping region of 2.4−2.0 V in the discharge curve is considered to represent the reduction

dx.doi.org/10.1021/jp400153m | J. Phys. Chem. C 2013, 117, 4431−4440

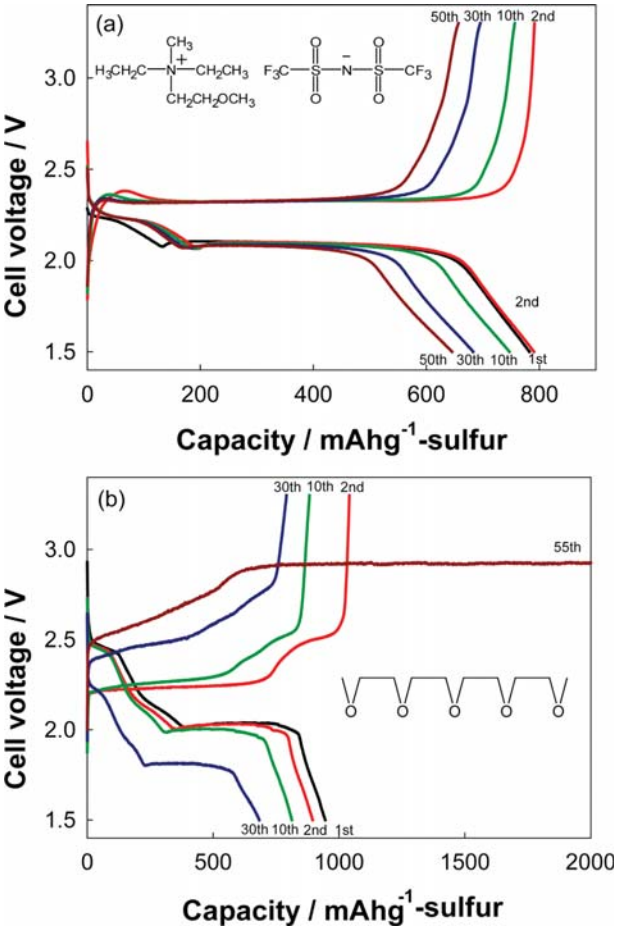

Figure 1. Galvanostatic charge–discharge curves of Li–S cells with (a) 0.64 M Li[TFSA]/[DEME][TFSA] and (b) 0.98 M Li[TFSA]/TEGDME measured at a current density of 139 mA g^{-1} sulfur at 30 °C. The structures of [DEME][TFSA] and TEGDME are shown in the insets.

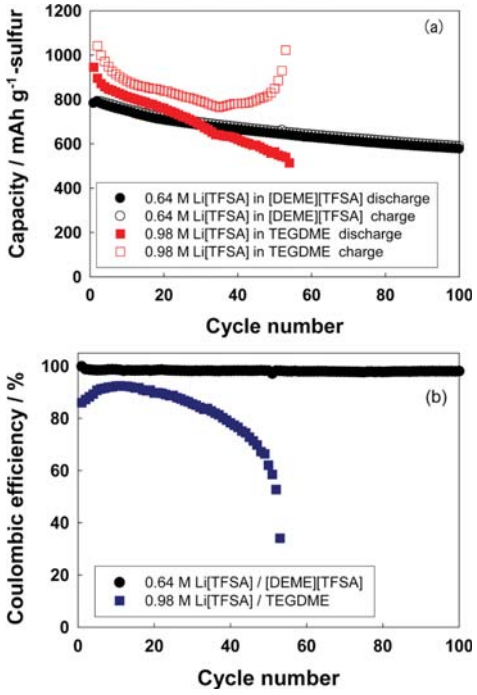

Figure 2. (a) Discharge–charge capacities and (b) Coulombic efficiency of Li–S cells with 0.64 M Li[TFSA]/[DEME][TFSA] and 0.98 M Li[TFSA]/TEGDME measured at a current density of 139 mA g^{-1} sulfur at 30 °C.

of S_8 into Li_2S_m (typically $m = 4$) through the formation of Li_2S_8.[12] A voltage plateau at around 2.0 V is ascribed to the reduction of Li_2S_4 into Li_2S. The charge profiles can be seen to change depending on the electrolyte composition. During the charge process, the cell with 0.64 M Li[TFSA]/[DEME]-[TFSA] shows a single voltage plateau at 2.3 V, while the cell with 0.98 M Li[TFSA]/TEGDME shows a voltage plateau at 2.2 V and a voltage-sloping region of 2.2–2.5 V. The dependence of the charge–discharge profile on the electrolyte composition is discussed later in this article.

The main differences among Li–S cells with different electrolytes were the charge–discharge cycle stability and Coulombic efficiency (Figure 2). A cell with 0.64 M Li[TFSA]/[DEME][TFSA] maintains a Coulombic efficiency >97% over 100 cycles. On the other hand, the Coulombic efficiency of cells with 0.98 M Li[TFSA]/TEGDME rapidly decreases with an increase in the charge–discharge cycles. The lower Coulombic efficiency can be attributed to the occurrence of the redox shuttle mechanism of Li_2S_m within the cell during the charge and discharge processes. Li_2S_m, which is generated through a cathodic reaction of the C/S composite, dissolves into ether-based electrolytes.[3−8,18−20] The dissolved Li_2S_m can diffuse from the composite cathode to the Li metal anode. The Li_2S_m can be further reduced to Li_2S_l ($l < m$) on the Li surface, and Li_2S_l can diffuse back toward the composite cathode to be further reduced when the cell is discharging and oxidized when the cell is charging.[8] Therefore, soluble Li_2S_m behaves as a redox shuttle in the cell. This redox cycling between Li_2S_m and Li_2S_l during a charge–discharge cycle causes low Coulombic efficiency of the Li–S cell (a decrease in the discharge capacity and an increase in the charging capacity). The decrease in the Coulombic efficiency of the 0.98 M Li[TFSA]/TEGDME cell with an increase in cycle number suggests that the concentration of Li_2S_m in the electrolyte increases with the cycle number. On the other hand, the cell with 0.64 M Li[TFSA]/[DEME][TFSA] can retain high Coulombic efficiency. Therefore, we hypothesize that the solubility of Li_2S_m in an RTIL is very low, and the redox shuttle mechanism is efficiently inhibited.

Solubility of Lithium Polysulfides in Electrolytes. To confirm the aforementioned hypothesis, the solubility of Li_2S_m in the electrolytes was investigated. The Li_2S_m solutions were prepared through a direct reaction of S_8 with Li_2S, as reported by Rauh et al.[68]

$$8Li_2S + (m - 1)S_8 \rightarrow 8Li_2S_m$$

The electrolytes were saturated with Li_2S_m, and the polysulfides in the electrolytes were subsequently analyzed. The UV–vis spectra of [DEME][TFSA], 0.64 M Li[TFSA]/[DEME]-[TFSA], and 0.98 M Li[TFSA]/TEGDME saturated with Li_2S_m are shown in Figure 3. The spectra of each electrolyte changed depending on the mixing ratio of S_8/Li_2S. Li_2S was almost insoluble in both the RTIL and TEGDME electrolytes. The peak assignments of the UV–vis spectra are not clear because the polysulfides formed in the electrolytes are a mixture of several species with different chain lengths owing to a

dx.doi.org/10.1021/jp400153m | J. Phys. Chem. C 2013, 117, 4431−4440

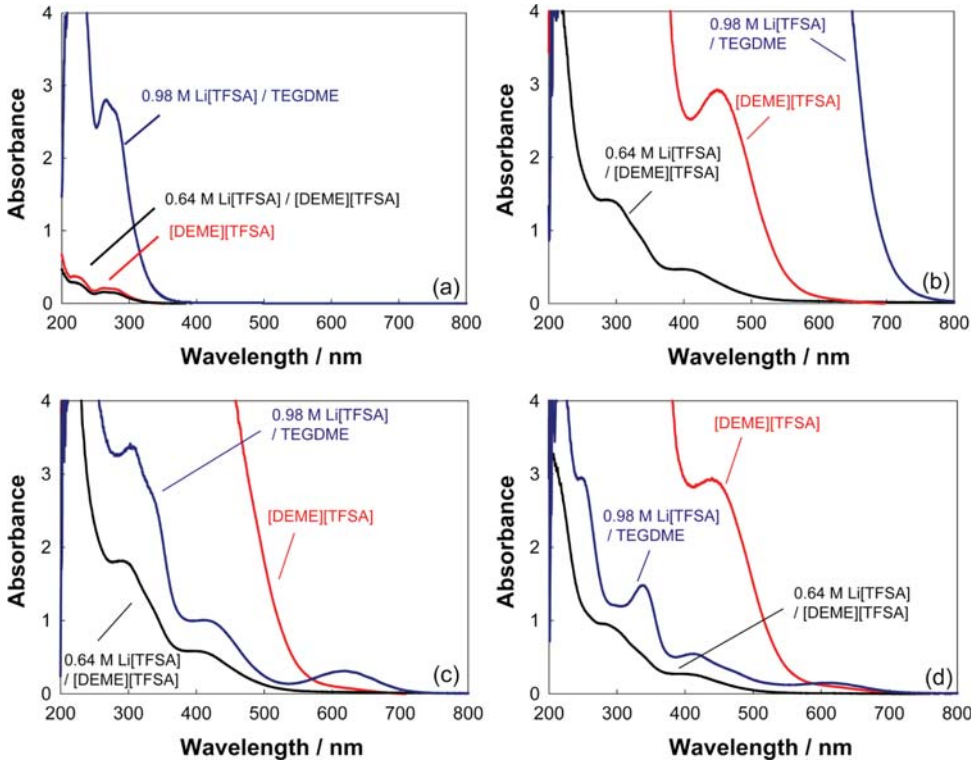

Figure 3. UV−vis spectra for electrolytes saturated with (a) S_8, (b) Li_2S_8, (c) Li_2S_4, and (d) Li_2S_2. The values of m in Li_2Sm are nominal, and the actual polysulfides in each electrolyte are mixtures of several species with different chain lengths.

disproportionation of S_m^{2-}.[71,72] However, it is clear that the polysulfide species changes depending on the electrolyte composition. For example, the peak at 620 nm, which has been assigned to an anion radical $S_3^{\bullet-}$ in previous reports,[71,72] was observed for 0.98 M Li[TFSA]/TEGDME solution; however, it did not appear in the spectra of 0.64 M Li[TFSA]/[DEME][TFSA]. This result clearly suggests that the dissolved polysulfide species changes depending on the type of electrolyte solvent used. Although the exact compositions of the polysulfide species in the electrolytes are difficult to determine precisely, the overall absorbance owing to the polysulfides in [DEME][TFSA] is larger than that in 0.64 M Li[TFSA]/[DEME][TFSA] in each sample shown in Figure 3, suggesting that the solubility of Li_2S_m is higher in [DEME]-[TFSA] without Li salt. These results suggest that the Li salt concentration in an electrolyte significantly affects the solubility of Li_2S_m.

To quantitatively evaluate the solubility of Li_2S_m in the electrolytes, Li_2S_m was electrochemically oxidized to S_8. The total S concentration was then determined by measuring the UV−vis spectra of the electrochemically oxidized solutions. Figure 4 shows the solubility limits of Li_2S_m in the electrolytes, presented as the total S concentration (in units of atomic concentration), which dramatically changes depending on the electrolyte composition. The solubility of Li_2S_m in Li[TFSA]/TEGDME is also shown for comparison. The solubility of Li_2S_m in 0.98 M Li[TFSA]/TEGDME solution is higher than that in Li[TFSA]/[DEME][TFSA] in every case. In particular, the total S concentration in the TEGDME solution, saturated at a mixed ratio of S_8/Li_2S = 7:8 (which corresponds to the average composition of Li_2S_8), is surprisingly higher than the concentrations in the other electrolytes. In contrast, the

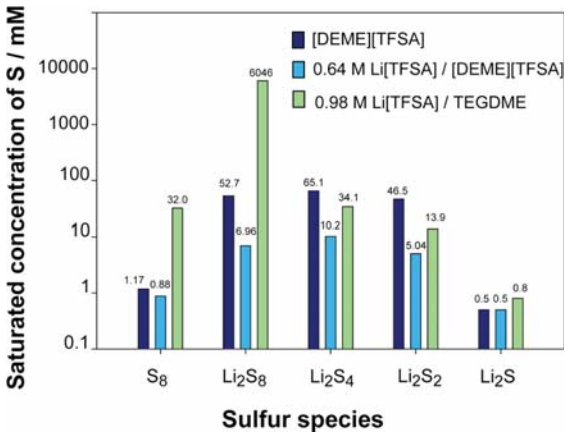

Figure 4. Solubility of S_8 and Li_2S_m in [DEME][TFSA], 0.64 M Li[TFSA]/[DEME][TFSA], and 0.98 M Li[TFSA]/TEGDME. The solubility is presented as the atomic concentration of S.

solubility of other forms of Li_2S_m with shorter chain lengths ($m \leq 4$) is less dependent on the electrolyte composition, suggesting that the length of the polysulfide anions has a significant effect on the solubility of Li_2S_m.

The solubility limit of Li_2S_8 in 0.64 M Li[TFSA]/[DEME][TFSA] is 6.96 mM (atomic concentration of S, corresponding to $[Li_2S_8]$ = 0.9 mM). On the other hand, the solubility limit of Li_2S_8 in a solution of 0.98 M Li[TFSA]/TEGDME is 6046 mM. It was reported that the solubility of Li_2S_m depends strongly on the donor ability of the solvent.[68] The Gutmann DN of TEGDME was reported to be 16.6,[54] which is a typical value for ether solvents, and the relatively

dx.doi.org/10.1021/jp400153m | J. Phys. Chem. C 2013, 117, 4431−4440

high DN indicates a high ability of TEGDME to dissolve the solutes. Indeed, organic solvents with a high DN such as DME, THF, and TEGDME can preferentially coordinate with Lewis acidic cations such as Li^+, which results in a high ability to dissociate alkali metal salts through strong solvation of cations. Thus, organic solvents with a high DN are frequently used as solvents for organic electrolytes in lithium batteries. Therefore, TEGDME with a relatively high DN dissolves Li_2S_m, as the electrostatic force between Li^+ and S_m^{2-} is not very strong when the S_m^{2-} chain length is relatively long, and TEGDME coordinates with the Li^+ cation and easily dissociates Li_2S_m. We assume that the origin of low solubility of Li_2S_m in Li[TFSA]/[DEME][TFSA] is the absence of a molecular solvent with high DN in the electrolyte. In addition, the $[TFSA]^-$ anion has weakly Lewis basic nature.[52] The maximum absorption wavelength (λ_{Cu}) of a solvatochromic probe [Cu(acac)(tmen)][BPh_4] is known to correlate well with the DN of the molecular solvents, where a higher λ_{Cu} indicates a stronger donor.[67] The λ_{Cu} values of pure [DEME][TFSA] and 0.64 M Li[TFSA]/[DEME][TFSA] were estimated to be 546 and 543 nm, respectively, which correspond to a DN of ca. 10. Therefore, the donating ability of a $[TFSA]^-$ anion is weaker than TEGDME, resulting in a low ability of 0.64 M Li[TFSA]/[DEME][TFSA] to dissolve Li_2S_m. λ_{Cu} of 0.64 M Li[TFSA]/[DEME][TFSA] is slightly smaller than that of pure [DEME]-[TFSA], indicating that the donor ability of [DEME][TFSA] is weakened by the addition of Li[TFSA]. By dissolving a Li salt into [DEME][TFSA], the coordination of Li^+ cations with two $[TFSA]^-$ anions and the formation of Li(I) oligomeric species occurs owing to the strong Lewis acidity of Li^+ cations (*vide supra*).[69,70] It is clear that the formation of complex structures between Li^+ and $[TFSA]^-$ weakens the donor ability of $[TFSA]^-$. In fact, the solubility of Li_2S_m in 0.64 M Li[TFSA]/[DEME][TFSA] is smaller than that in pure [DEME][TFSA] (Figure 4).

The electrolyte used in batteries was incorporated into a porous separator, which limited the available volume of electrolyte to its void volume. In this study, a [Lilelectrolyte with a glass separator|C/S] coin cell was used. The volume of the electrolyte was only ca. 36 μL, and the mass of S in the C/S composite cathode was 1.2 mg. When 0.64 M Li[TFSA]/[DEME][TFSA] in the coin cell was saturated with the electrochemically generated Li_2S_8, 8.0 μg of S_m^{2-} was dissolved in the electrolyte, corresponding to ca. 0.7% of S being incorporated into the initial C/S composite electrode. Therefore, the majority of the electrochemically generated Li_2S_m should be in solid state and remain in the C pores. The [Li|0.64 M Li[TFSA]/[DEME][TFSA]|C/S] cell exhibited a good Coulombic efficiency of higher than 97% during 100 cycles. It is evident that the diffusion of Li_2S_m is intrinsically suppressed in 0.64 M Li[TFSA]/[DEME][TFSA].

On the other hand, the reduction of S in a Li–S cell with 0.98 M Li[TFSA]/TEGDME electrolyte involves the conversion of solid S_8 to soluble Li_2S_8. The effect of the redox shuttle mechanism resulting from the dissolved Li_2S_m is more clearly observed with a repeating charge–discharge cycle in 0.98 M Li[TFSA]/TEGDME. As shown in Figure 2, the redox shuttle mechanism causes progressive increase and decrease in the charge and discharge capacities, respectively. It can be concluded that the dissolution of Li_2S_m is high in a cell with 0.98 M Li[TFSA]/TEGDME solution.

Charge–Discharge Mechanisms of Li–S Cells. GITT was used to study the electrochemical behavior of S electrode in further detail. Figure 5 shows the GITT profiles of [Lil electrolytelC/S] cells. As represented by the circles in the figure, the OCV for each cell during the discharge process has two voltage regions similar to galvanostatic discharge curves (Figure 1), namely, a high-voltage region of 2.4–2.0 V and a low-voltage plateau of 2.0 V. As shown in the GITT profile in the high-voltage region of the discharge, the voltage change during relaxation is small, indicating that the overvoltage for the electrochemical reaction is small and that the electrode kinetics is relatively fast. However, a larger polarization is observed at the end of the lower voltage region. This can be explained by the slow kinetics of the solid-state reaction of $Li_2S_m \rightarrow Li_2S$ and by an increase in the mass-transport resistance in the pores of the composite cathode. Although galvanostatic titration was carried out with a small current of 139 mA g^{-1}, the theoretical capacity of 1672 mA h g^{-1} sulfur was not achieved. It is likely that the low electronic conductivity of S_8 and Li_2S_m and the volume change of the active material during the discharge reaction cause low utilization of the active material. The low electronic conductivity easily produces a nonaccessible active material in the C/S composite cathodes. Further, the densities of S_8 and Li_2S are 2.07 and 1.66 g cm^{-3}, respectively, and the volume of the active material becomes ~1.8 times larger during the electrochemical reaction, $S_8 \rightarrow 8Li_2S$. Owing to the volume change, the pores of the C/S composite may be filled,[73] and the ionic conduction path within the composite electrode may be blocked. This blockage brings about an end of the discharge before attaining complete utilization of the active material. Interestingly, as decreasing the mass ratio of S in C/S composite, the specific discharge capacity based on the mass of S was increased (data not shown). The porosity of the composite is increased as decreasing the mass ratio of S. The

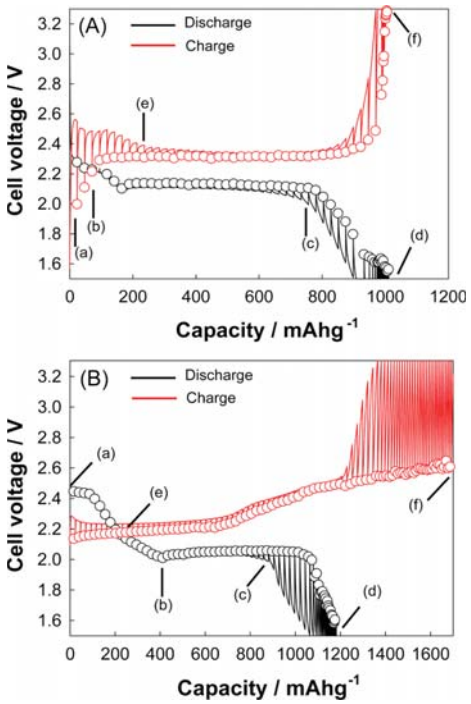

Figure 5. GITT profiles of Li–S cells with (A) 0.64 M Li[TFSA]/[DEME][TFSA] and (B) 0.98 M Li[TFSA]/TEGDME. The circles denote the OCV at each charge or discharge state of Li–S cells.

dx.doi.org/10.1021/jp400153m | J. Phys. Chem. C 2013, 117, 4431–4440

large porosity provides sufficient ionic conduction path within the composite electrode and allows volume expansion of active material during the electrochemical reaction of $S_8 \rightarrow 8Li_2S$. This consideration agrees with the report by Li et al.[73]

The volume change owing to the conversion reaction of $S_8 \rightarrow 8Li_2S$ may also be responsible for the capacity fade of Li−S cell during charge−discharge cycling. The capacity of a cell with 0.64 M Li[TFSA]/[DEME][TFSA] gradually decreases with an increase in the number of cycles, regardless of the high Coulombic efficiency of the discharge/charge (Figure 2). A volume change of the active material may loosen the electrical contact between the C support and the active material and may isolate S from the C support. The isolated S cannot participate in the redox reaction, and the capacity degradation of the cell results in. An optimization of the porous structure of a C/S composite electrode may be necessary to achieve long-term cycle stability. Many excellent studies have been conducted on the architecture of C/S composite electrodes,[66,73−85] and an optimized C/S electrode will be helpful in achieving higher performance of Li−S cells with RTILs.

The high-voltage regions of OCV for cells with 0.64 M Li[TFSA]/[DEME][TFSA] and 0.98 M Li[TFSA]/TEGDME were observed during the discharge at around 2.3 and 2.5 V, respectively (Figure 5). This OCV difference reflects the difference in the electrochemical reaction mechanisms. We assume that the following reaction takes place in the high-voltage region:

$$2Li + S_8 \rightarrow Li_2S_8$$

The electromotive force (ΔE°) of a Li−S cell under standard conditions can be written as follows:

$$-nF\Delta E^\circ = \Delta_f G(Li_2S_8) - \Delta_f G(S_8) - 2\Delta_f G(Li)$$
$$= \Delta_f G(Li_2S_8)$$

where n is the number of transferred electrons ($n = 2$), F is the Faraday constant, and $\Delta_f G(Li_2S_8)$, $\Delta_f G(S_8)$, and $\Delta_f G(Li)$ are the standard Gibbs free energy change of formation of Li_2S_8, S_8, and Li, respectively. In the RTIL, the majority of Li_2S_8 remained in solid state, whereas most of the compound dissolved into 0.98 M Li[TFSA]/TEGDME solution (*vide supra*). Herein, $\Delta_f G(Li_2S_8$, solvated) and $\Delta_f G(Li_2S_8$, solid) are the Gibbs free energy change of formation for solvated Li_2S_8 and solid-state Li_2S_8, respectively, and their relation should be $\Delta_f G(Li_2S_8$, solvated) < $\Delta_f G(Li_2S_8$, solid). The Gibbs free energy change for the dissolution of Li_2S_8 (= $\Delta_f G(Li_2S_8$, solvated) − $\Delta_f G(Li_2S_8$, solid)) can be roughly estimated from the OCV difference between the cells with 0.64 M Li[TFSA]/[DEME][TFSA] and the cells with 0.98 M Li[TFSA]/TEGDME, based on the assumption that each OCV is equal to the electromotive force of each cell at equilibrium. When the discharge capacity of each cell reached 100 mA h g^{-1} S, the OCV difference between the cells with 0.64 M Li[TFSA]/[DEME][TFSA] and the cells with 0.98 M Li[TFSA]/TEGDME was ca. 0.2 V. The concentration of Li_2S_8 in 0.98 M Li[TFSA]/TEGDME at a discharged state of 100 mA h g^{-1} was estimated to be 62 mM (corresponding to 496 mM atomic concentration of S), which was calculated from the initial mass of the active material (1.2 mg) and the electrolyte volume (36 μL). According to the solubility of Li_2S_8, as shown in Figure 4, all of the electrochemically generated Li_2S_8 in the cell should dissolve into the 0.98 M Li[TFSA]/TEGDME electrolyte. Taking into account the concentrations of Li_2S_8 and Li[TFSA] in the electrolytes, the Gibbs free energy change for the dissolution of Li_2S_8 was roughly estimated to be −37 kJ mol^{-1}. This estimation supports the hypothesis that Li_2S_8 is stabilized through solvation and can be easily dissolved in TEGDME solvent. On the other hand, the binary ionic liquid Li[TFSA]/[DEME][TFSA] thermodynamically suppresses the dissolution of Li_2S_m owing to the absence of a molecular solvent. The equilibrium solubility of Li_2S_m changes depending on the electrolyte composition, and the electrochemical reaction mechanism of the S cathode greatly changes depending on the electrolyte solvent used. In other words, this result demonstrates a *solvent effect* of RTILs on a S-cathode reaction.

To assess the solubility of Li_2S_m during an electrochemical reaction within the Li−S cells, the cells were disassembled at various discharged states. The disassembly of each cell was carried out in an Ar-filled glovebox to avoid the moisture reaction of Li_2S_m. The dissolved Li_2S_m diffused from the S cathode into the electrolyte supported in a porous separator within the cell. To extract the dissolved Li_2S_m, the separator was removed from the cell and soaked in 0.5 mL of fresh electrolyte with the same composition. Figure 6 shows the UV−vis spectra

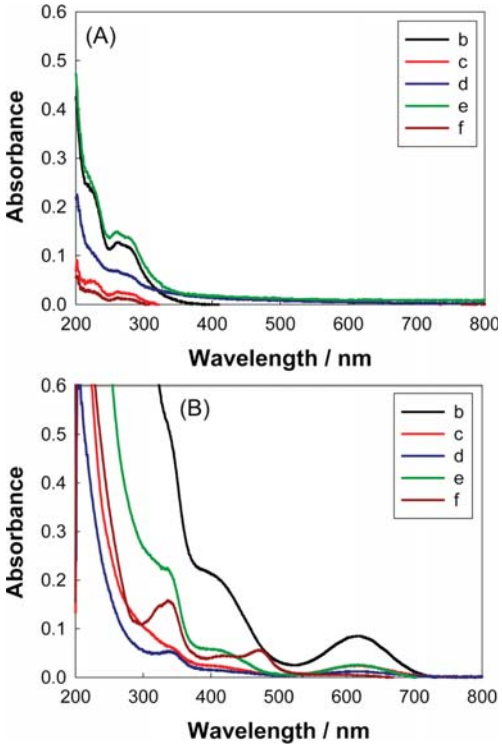

Figure 6. UV−vis spectra for electrolytes sampled from Li−S cells during the discharge processes. Electrolytes: (A) 0.64 M Li[TFSA]/[DEME][TFSA] and (B) 0.98 M Li[TFSA]/TEGDME. In (A) and (B), (b)−(f) correspond to the discharged states of the Li−S cells shown in Figure 5.

of dissolved Li_2S_m from the Li−S cells. The absorbance of the analyte solutions in 0.98 M Li[TFSA]/TEGDME is much higher than that in 0.64 M Li[TFSA]/[DEME][TFSA], indicating the higher solubility of Li_2S_m in the Li[TFSA]/TEGDME solution, which is in good agreement with the results shown in Figure 4. Note that the UV−vis spectra of the solutions extracted from the separator are similar to those of the Li_2S_m solutions prepared by a direct reaction between Li_2S

dx.doi.org/10.1021/jp400153m | J. Phys. Chem. C 2013, 117, 4431−4440

and S_8 (Figure 3). As can be seen in the spectra, the absorbance of Li_2S_m in each electrolyte at the initial stage of discharge (Figures 6Ab and 6Bb) is higher than for the other stages because the solubility of Li_2S_8 is much higher than that of other forms of Li_2S_m ($1 \leq m \leq 4$) (Figure 4). The absorbance caused by Li_2S_m decreases as the discharge progresses. This suggests that the dissolved Li_2S_m is electrochemically reduced to an insoluble Li_2S_m species at the cathode; therefore, the cathode was subjected to XRD measurements. The diffraction peak due to Li_2S began to appear at the 2 V plateau and became pronounced with an increase in the depth of discharge (DOD) (Figure 7), suggesting that insoluble Li_2S is produced at the 2 V plateau of the discharge process.

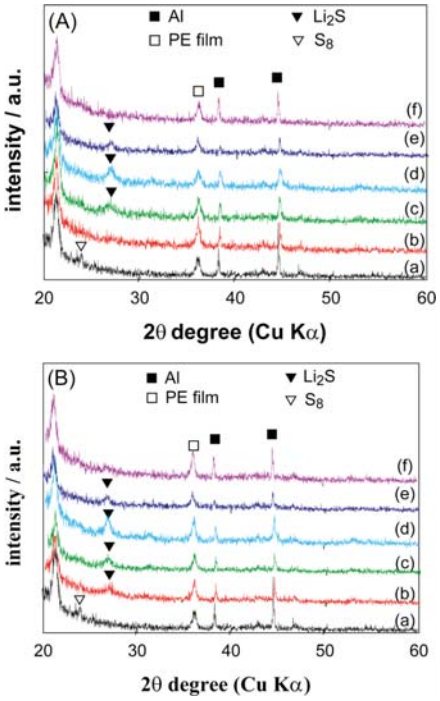

Figure 7. XRD patterns of C/S composite cathodes obtained from cells with electrolytes of (A) 0.64 M Li[TFSA]/[DEME][TFSA] and (B) 0.98 M Li[TFSA]/TEGDME. In (A) and (B), (a)−(f) correspond to the discharged states of Li−S cells shown in Figure 5.

In contrast to the two voltage regions appearing in the OCV profile of the discharge process, the charge process exhibits only one voltage region in 0.64 M Li[TFSA]/[DEME][TFSA]. Although the origin of this hysteresis is unclear, there is a possibility that a direct solid-phase-conversion reaction from Li_2S to S_8 occurs and that the slow kinetics of the electrochemical reaction in the low-voltage region of the discharge may induce certain mixed potential conditions during the charging process.

The GITT profile measured during the charging of a cell with the 0.98 M Li[TFSA]/TEGDME solution exhibits two voltage regions: a 2.25 V plateau and a voltage-sloping region of 2.25−2.6 V (Figure 5B), which is similar to the profile observed during the discharge process. In the voltage region above 2.5 V, the overvoltage for the electrochemical reaction increases; however, the OCV remains below 2.6 V, and the total charge capacity exceeds the theoretical capacity of 1672 mA h g^{-1}. This phenomenon can be attributed to the redox shuttle mechanism owing to the dissolved Li_2S_m (*vide supra*). From the GITT profile, it is postulated that the redox shuttle mechanism occurs mainly in the high-voltage region (2.4−2.0 V for the discharge process and 2.25−2.6 V for the charge process) owing to the high shuttle concentration (Li_2S_m) in the electrolyte.

Discharge Rate Capability of Li−S Cell with RTIL. As demonstrated, the charge and discharge reactions of the C/S composite electrode in 0.64 M Li[TFSA]/[DEME][TFSA] take place almost completely in the solid state, while the charge and discharge in 0.98 M Li[TFSA]/TEGDME solution involve the dissolution and precipitation processes of Li_2S_m. The suppressed solubility of Li_2S_m in the RTIL results in a high Coulombic efficiency and cycle stability of the Li−S cell. The electrode kinetics of S cathode is also an important factor in constructing a high-performance device. To understand the electrode kinetics, we discharged Li−S cells at various current densities. Figure 8 shows the discharge rate capability of Li−S

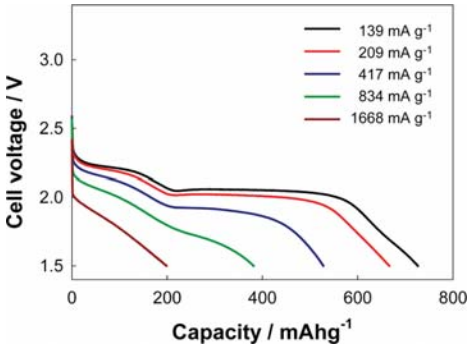

Figure 8. Discharge curves of Li−S cell with 0.64 M Li[TFSA]/[DEME][TFSA] measured at various current densities at 30 °C. Prior to each discharge, the cell was charged up to 3.3 V at a current density of 139 mA g^{-1} sulfur.

cells with 0.64 M Li[TFSA]/[DEME][TFSA]. The discharge capacity of the cell decreases with an increase in the current density, which can be attributed to the slow kinetics of the electrochemical reaction of solid state Li_2S_m and the mass-transport resistance of the electrolyte within the porous C/S composite electrode structure. The reduction kinetics of Li_2S_m at the 2 V plateau was clearly slower than in the voltage region of 2.4−2 V. The discharge capacity at the 2 V plateau rapidly deteriorates with an increase in the current density, while the capacity in the 2.4−2 V region is nearly independent of the current density. The resistance of the C/S electrode is enhanced with an increase in the DOD. A larger overvoltage is needed at a higher DOD, as can be seen in the GITT profile (Figure 5). The mass-transport resistance of an electrolyte within a porous C/S composite electrode structure should increase with an increase in the DOD.[73] In addition, the kinetics of a solid-state redox reaction of Li_2S_m may become sluggish by shortening the chain length of S_m^{2-}.[2] Optimization of the porous structure of a C/S composite electrode may be necessary to achieve a high discharge rate capability of Li−S cell. The nanoarchitecture of C/S may be effective in collecting a faradaic current from an active material efficiently and in enhancing the mass transport of the electrolyte within an electrode.[66,73−85]

dx.doi.org/10.1021/jp400153m | J. Phys. Chem. C 2013, 117, 4431−4440

CONCLUSIONS

A binary RTIL (Li[TFSA]/[DEME][TFSA]) was used as an electrolyte for Li−S cell. The solubility of Li_2S_m ($2 \leq m \leq 8$) in the RTIL was greatly suppressed as compared with a conventional electrolyte of Li[TFSA]/TEGDME. It was revealed that the RTIL has low donor ability owing to the weak Lewis basicity of a $[TFSA]^-$ anion, resulting in very poor solubility of Li_2S_m. Using the RTIL, the redox shuttle mechanism during the charge−discharge cycle of Li−S cell was suppressed owing to the very small concentration of Li_2S_m in the electrolyte. This leads to a higher Coulombic efficiency and longer cycle life of Li−S cell. Both S_8 and Li_2S_m in the RTIL were immobilized in the electrode, and an electrochemical reaction of the S species occurred exclusively in the solid phase. This behavior is in contrast to that occurring in Li[TFSA]/TEGDME electrolyte, where the dissolution and precipitation of Li_2S_m take place during the discharge and charge. These results clearly prove the existence of a *solvent effect* of RTILs on the electrochemical reaction of S cathode in Li−S cells. The electrochemical reaction resistance of the C/S composite cathode increases with increase in the DOD owing to the volume increase of the active material during the electrochemical reaction $S_8 \rightarrow 8Li_2S$, which increases mass-transport resistance within the pores of the composite cathode.

ASSOCIATED CONTENT

Supporting Information

Estimation of energy density of Li−S cells. This material is available free of charge via the Internet at http://pubs.acs.org.

AUTHOR INFORMATION

Corresponding Author

*Fax +81-45-339-3955; e-mail mwatanab@ynu.ac.jp.

Notes

The authors declare no competing financial interest.

ACKNOWLEDGMENTS

This study was supported in part by the Advanced Low Carbon Technology Research and Development Program (ALCA) of the Japan Science and Technology Agency (JST) and by the Technology Research Grant Program from the New Energy and Industrial Technology Development Organization (NEDO) of Japan.

REFERENCES

(1) Bruce, P. G.; Freunberger, S. A.; Hardwick, L. J.; Tarascon, J.-M. *Nat. Mater.* **2012**, *11*, 19.
(2) Ellis, B. L.; Lee, K. T.; Nazar, L. F. *Chem. Mater.* **2010**, *22*, 691.
(3) Rauh, R. D.; Abraham, K. M.; Pearson, G. F.; Surprenant, J. K.; Brummer, S. B. *J. Electrochem. Soc.* **1979**, *126*, 523.
(4) Yamin, H.; Peled, E. *J. Power Sources* **1983**, *9*, 281.
(5) Peled, E.; Gorenshtein, A.; Segal, M.; Sternberg, Y. *J. Power Sources* **1989**, *26*, 269.
(6) Cheon, S.-E.; Ko, K.-S.; Cho, J.-H.; Kim, S.-W.; Chin, E.-Y.; Kim, H.-T. *J. Electrochem. Soc.* **2003**, *150*, A800.
(7) Ryu, H. S.; Guo, Z.; Ahn, H. J.; Cho, G. B.; Liu, H. *J. Power Sources* **2009**, *189*, 1179.
(8) Mikhaylik, Y. V.; Akridge, J. R. *J. Electrochem. Soc.* **2004**, *151*, A1969.
(9) Ji, X.; Lee, K. T.; Nazar, L. F. *Nat. Mater.* **2009**, *8*, 500.
(10) Ji, X.; Nazar, L. F. *J. Mater. Chem.* **2010**, *20*, 9821.
(11) Ji, X.; Evers, S.; Black, R.; Nazar, L. F. *Nat. Commun.* **2011**, *2*, 325.
(12) Jeong, S. S.; Lim, Y. T.; Choi, Y. J.; Cho, G. B.; Kim, K. W.; Ahn, H. J.; Cho, K. K. *J. Power Sources* **2007**, *174*, 745.
(13) Marmorstein, D.; Yu, T. H.; Striebel, K. A.; McLarnon, F. R.; Hou, J.; Cairns, E. J. *J. Power Sources* **2000**, *89*, 219.
(14) Ryu, H.-S.; Ahn, H.-J.; Kim, K.-W.; Ahn, J.-H.; Lee, J.-Y. *J. Power Sources* **2006**, *153*, 360.
(15) Wang, J. L.; Yang, J.; Xie, J. Y.; Xu, N. X.; Li, Y. *Electrochem. Commun.* **2002**, *4*, 499.
(16) Hayashi, A.; Ohtomo, T.; Mizuno, F.; Tadanaga, K.; Tatsumisago, M. *Electrochem. Commun.* **2003**, *5*, 701.
(17) Kobayashi, T.; Imade, Y.; Shishihara, D.; Homma, K.; Nagao, N.; Watanabe, R.; Yokoi, T.; Yamada, A.; Kanno, R.; Tatsumi, T. *J. Power Sources* **2008**, *182*, 621.
(18) Yamin, H.; Penciner, J.; Gorenshtain, A.; Elam, M.; Peled, E. *J. Power Sources* **1985**, *14*, 129.
(19) Yamin, H.; Gorenshtein, A.; Penciner, J.; Sternberg, Y.; Peled, E. *J. Electrochem. Soc.* **1988**, *135*, 1045.
(20) Peled, E.; Sternberg, Y.; Gorenshtein, A.; Lavi, Y. *J. Electrochem. Soc.* **1989**, *136*, 1621.
(21) Choi, J.-W.; Kim, J.-K.; Cheruvally, G.; Ahn, J.-H.; Ahn, H.-J.; Kim, K.-W. *Electrochim. Acta* **2007**, *52*, 2075.
(22) Shin, J. H.; Cairns, E. J. *J. Electrochem. Soc.* **2008**, *155*, A368.
(23) Aurbach, D.; Pollak, E.; Elazari, R.; Salitra, G.; Kelley, C. S.; Affinito, J. *J. Electrochem. Soc.* **2009**, *156*, A694.
(24) Elazari, R.; Salitra, G.; Talyosef, Y.; Grinblat, J.; Scordilis-Kelley, C.; Xiao, A.; Affinito, J.; Aurbach, D. *J. Electrochem. Soc.* **2010**, *157*, A1131.
(25) Yuan, L. X.; Feng, J. K.; Ai, X. P.; Cao, Y. L.; Chen, S. L.; Yang, H. X. *Electrochem. Commun.* **2006**, *8*, 610.
(26) Wang, J.; Chew, S. Y.; Zhao, Z. W.; Ashraf, S.; Wexler, D.; Chen, J.; Ng, S. H.; Chou, S. L.; Liu, H. K. *Carbon* **2008**, *46*, 229.
(27) Welton, T. *Chem. Rev.* **1999**, *99*, 2071.
(28) Wasserscheid, P.; Keim, W. *Angew. Chem., Int. Ed.* **2000**, *39*, 3772.
(29) Seddon, K. R. *Nat. Mater.* **2003**, *2*, 363.
(30) Armand, M.; Endres, F.; MacFarlane, D. R.; Ohno, H.; Scrosati, B. *Nat. Mater.* **2009**, *8*, 621.
(31) Angell, C. A.; Ansari, Y.; Zhao, Z. F. *Faraday Discuss.* **2012**, *154*, 9.
(32) Sato, T.; Masuda, G.; Takagi, K. *Electrochim. Acta* **2004**, *49*, 3603.
(33) Ue, M.; Takeda, M.; Toriumi, A.; Kominato, A.; Hagiwara, R.; Ito, Y. *J. Electrochem. Soc.* **2003**, *150*, A499.
(34) Isshiki, Y.; Nakamura, M.; Tabata, S.; Dokko, K.; Watanabe, M. *Polym. Adv. Technol.* **2011**, *22*, 1254.
(35) Imaizumi, S.; Kato, Y.; Kokubo, K.; Watanabe, M. *J. Phys. Chem. B* **2012**, *116*, 5080.
(36) Kubo, W.; Kambe, S.; Nakade, S.; Kitamura, T.; Hanabusa, K.; Wada, Y.; Yanagida, S. *J. Phys. Chem. B* **2003**, *107*, 4374.
(37) Wang, P.; Zakeeruddin, S.; Moser, J.-E.; Grätzel, M. *J. Phys. Chem. B* **2003**, *107*, 13280.
(38) Kawano, R.; Katakabe, T.; Shimosawa, H.; Nazeeruddin, M. K.; Grätzel, M.; Matsui, H.; Kitamura, T.; Tanabe, N.; Watanabe, M. *Phys. Chem. Chem. Phys.* **2010**, *12*, 1916.
(39) Garcia, B.; Lavallée, S.; Perron, G.; Michot, C.; Armand, M. *Electrochim. Acta* **2004**, *49*, 4583.
(40) Shin, J.-H.; Henderson, W. A.; Passerini, S. *J. Electrochem. Soc.* **2005**, *152*, A978.
(41) Matsumoto, H.; Sakaebe, H.; Tatsumi, K. *J. Power Sources* **2005**, *146*, 45.
(42) Matsumoto, H.; Sakaebe, H.; Tatsumi, K.; Kikuta, M.; Ishiko, E.; Kono, M. *J. Power Sources* **2006**, *160*, 1308.
(43) Fernicola, A.; Croce, F.; Scrosati, B.; Watanabe, T.; Ohno, H. *J. Power Sources* **2007**, *174*, 342.
(44) Seki, S.; Kobayashi, Y.; Miyashiro, H.; Ohno, Y.; Usami, A.; Mita, Y.; Kihira, N.; Watanabe, M.; Terada, N. *J. Phys. Chem. B* **2006**, *110*, 10228.

(45) Seki, S.; Ohno, Y.; Kobayashi, Y.; Miyashiro, H.; Usami, A.; Mita, Y.; Tokuda, H.; Watanabe, M.; Hayamizu, K.; Tsuzuki, S.; Hattori, M.; Terada, N. *J. Electrochem. Soc.* **2007**, *154*, A173.
(46) Park, J.-W.; Yoshida, K.; Tachikawa, N.; Dokko, K.; Watanabe, M. *J. Power Sources* **2011**, *196*, 2264.
(47) Yoshida, K.; Tsuchiya, M.; Tachikawa, N.; Dokko, K.; Watanabe, M. *J. Electrochem. Soc.* **2012**, *159*, A1005.
(48) Ueno, K.; Tokuda, H.; Watanabe, M. *Phys. Chem. Chem. Phys.* **2010**, *12*, 1649.
(49) Tokuda, H.; Hayamizu, K.; Ishii, K.; Susan, M. A. B. H.; Watanabe, M. *J. Phys. Chem. B* **2004**, *108*, 16593.
(50) Tokuda, H.; Hayamizu, K.; Ishii, K.; Susan, M. A. B. H.; Watanabe, M. *J. Phys. Chem. B* **2005**, *109*, 6103.
(51) Tokuda, H.; Ishii, K.; Susan, M. A. B. H.; Tsuzuki, S.; Watanabe, M. *J. Phys. Chem. B* **2006**, *110*, 2833.
(52) Tokuda, H.; Tsuzuki, S.; Susan, M. A. B. H.; Hayamizu, K.; Watanabe, M. *J. Phys. Chem. B* **2006**, *110*, 19593.
(53) Brouillette, D.; Irish, D. E.; Taylor, N. J.; Perron, G.; Odziemkowski, M.; Desnoyers, J. E. *Phys. Chem. Chem. Phys.* **2002**, *4*, 6063.
(54) Brouillette, D.; Perron, G.; Desnoyers, J. E. *J. Solution Chem.* **1998**, *27*, 151.
(55) Henderson, W. A.; Brooks, N. R.; Brennessel, W. W.; Young, V. G., Jr. *Chem. Mater.* **2003**, *15*, 4679.
(56) Henderson, W. A.; Brooks, N. R.; Young, V. G., Jr. *Chem. Mater.* **2003**, *15*, 4685.
(57) Henderson, W. A.; Mckenna, F.; Kahn, M. A.; Brooks, N. R.; Young, V. G., Jr.; Frech, R. *Chem. Mater.* **2005**, *17*, 2284.
(58) Henderson, W. A. *J. Phys. Chem. B* **2006**, *110*, 13177.
(59) Zhang, C.; Ainsworth, D.; Andreev, Y. G.; Bruce, P. G. *J. Am. Chem. Soc.* **2007**, *129*, 8700.
(60) Zhang, C.; Andreev, Y. G.; Bruce, P. G. *Angew. Chem., Int. Ed.* **2007**, *46*, 2848.
(61) Zhang, C.; Lilley, S. J.; Ainsworth, D.; Staunton, E.; Andreev, Y. G.; Slawin, A. M. Z.; Bruce, P. G. *Chem. Mater.* **2005**, *17*, 2284.
(62) Ueno, K.; Yoshida, K.; Tsuchiya, M.; Tachikawa, N.; Dokko, K.; Watanabe, M. *J. Phys. Chem. B* **2012**, *116*, 11323.
(63) Yoshida, K.; Nakamura, M.; Kazue, Y.; Tachikawa, N.; Tsuzuki, S.; Seki, S.; Dokko, K.; Watanabe, M. *J. Am. Chem. Soc.* **2011**, *133*, 13121.
(64) Yoshida, K.; Tsuchiya, M.; Tachikawa, N.; Dokko, K.; Watanabe, M. *J. Phys. Chem. C* **2011**, *115*, 18384.
(65) Tamura, T.; Yoshida, K.; Hachida, T.; Tsuchiya, M.; Nakamura, M.; Kazue, Y.; Tachikawa, N.; Dokko, K.; Watanabe, M. *Chem. Lett.* **2010**, *39*, 753.
(66) Tachikawa, N.; Yamauchi, K.; Takashima, E.; Park, J.-W.; Dokko, K.; Watanabe, M. *Chem. Commun.* **2011**, *47*, 8157.
(67) Muldoon, M. J.; Gordon, C. M.; Dunkin, I. R. *J. Chem. Soc., Perkin Trans. 2* **2001**, 433.
(68) Rauh, R. D.; Shuker, F. S.; Marston, J. M.; Brummer, S. B. *J. Inorg. Nucl. Chem.* **1977**, *39*, 1761.
(69) Shirai, A.; Fujii, K.; Seki, S.; Umebayashi, Y.; Ishiguro, S.; Ikeda, Y. *Anal. Sci.* **2008**, *24*, 1291.
(70) Umebayashi, Y.; Mori, S.; Fujii, K.; Tsuzuki, S.; Seki, S.; Hayamizu, K.; Ishiguro, S. *J. Phys. Chem. B* **2010**, *114*, 6513.
(71) Tobishima, S.-I.; Yamamoto, H.; Matsuda, M. *Electrochim. Acta* **1997**, *42*, 1019.
(72) Manan, N. S. A.; Aldous, L.; Alias, Y.; Murray, P.; Yellowlees, L. J.; Lagunas, M. C.; Hardacre, C. *J. Phys. Chem. B* **2011**, *115*, 13873.
(73) Li, X.; Cao, Y.; Qi, W.; Saraf, L. V.; Xiao, J.; Nie, Z.; Mietek, J.; Zhang, J.-G.; Schwenzer, B.; Liu, J. *J. Mater. Chem.* **2011**, *21*, 16603.
(74) Liang, C.; Dudney, N. J.; Howe, J. Y. *Chem. Mater.* **2009**, *21*, 4724.
(75) Hassoun, J.; Scrosati, B. *Angew. Chem., Int. Ed.* **2010**, *49*, 2371.
(76) Han, S.-C.; Song, M.-S.; Lee, H.; Kim, H.-S.; Ahn, H.-J.; Lee, J.-Y. *J. Electrochem. Soc.* **2003**, *150*, A889.
(77) Wang, J.-Z.; Lu, L.; Choucair, M.; Stride, J. A.; Xu, X.; Liu, H.-K. *J. Power Sources* **2011**, *196*, 7030.
(78) Wang, H.; Yang, Y.; Liang, Y.; Robinson, J. T.; Li, Y.; Jackson, A.; Cui, Y.; Dai, H. *Nano Lett.* **2011**, *11*, 2644.
(79) Zheng, G.; Yang, Y.; Cha, J. J.; Hong, S. S.; Cui, Y. *Nano Lett.* **2011**, *11*, 4462.
(80) Lai, C.; Gao, X. P.; Zhang, B.; Yan, T. Y.; Zhou, Z. *J. Phys. Chem. C* **2009**, *113*, 4712.
(81) Jayaprakash, N.; Shen, J.; Moganty, S. S.; Corona, A.; Archer, L. A. *Angew. Chem., Int. Ed.* **2011**, *50*, 5904.
(82) Demir-Cakan, R.; Morcrette, M.; Nouar, F.; Davoisne, C.; Devic, T.; Gonbeau, D.; Dominko, R.; Serre, C.; Férey, G.; Tarascon, J.-M. *J. Am. Chem. Soc.* **2011**, *133*, 16154.
(83) Wu, F.; Chen, J.; Chen, R.; Wu, S.; Li, L.; Chen, S.; Zhao, T. *J. Phys. Chem. C* **2011**, *115*, 6057.
(84) Qiu, L.; Zhang, S.; Zhang, L.; Sun, M.; Wang, W. *Electrochim. Acta* **2010**, *55*, 4632.
(85) Yang, Y.; Yu, G.; Cha, J. J.; Wu, H.; Vosgueritchian, M.; Yao, Y.; Bao, Z.; Cui, Y. *ACS Nano* **2011**, *5*, 9187.